

# THE ROTORDYNAMIC INTEGRITY OF A NEW MACHINE— A VERTICAL HYDRAULIC TURBINE IN CRYOGENIC FLUIDS

by

**Gilbert L.G.M. Habets**

Shell International Oil Products B.V.

The Hague, The Netherlands

and

**Anthony J. Smalley**

Institute Engineer

Southwest Research Institute

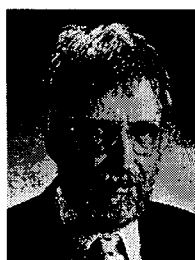
San Antonio, Texas



*Gilbert L.G.M. Habets began as a Mechanical Engineer with ARAMCO Overseas Company in The Hague, The Netherlands. His career has included work with ARAMCO in Dhahran, Saudi Arabia, Shell International in The Hague, research in Amsterdam, chemical plants in The Netherlands, and the Al Jubail Refinery in Saudi Arabia. In 1987, he was assigned to Woodside Energy Limited in Western Australia and worked on their new liquefied*

*natural gas plant. After returning to Shell in The Hague, he was assigned to several design teams for new LNG and refinery projects in the Far East, Middle East, and Australia. His last assignment in 1999 was with Reliance in India on the startup and maintenance of their massive Greenfield Refinery. He has published several papers, and is a member of ASME and Australian Institute of Engineers.*

*Mr. Habets received his M.S. degree (Mechanical Engineering, 1978) from the Technical University in Eindhoven, The Netherlands.*



*Anthony J. (Tony) Smalley is an Institute Engineer in the Mechanical and Materials Engineering Division at Southwest Research Institute, in San Antonio, Texas. He has more than 30 years' experience in problem solving in machinery dynamics and performance. Dr. Smalley has made technical contributions in the control of vibrations, the analysis of bearings, the design of foundations, machinery condition monitoring, and diagnostics. He has*

*worked on machinery and plants used by gas transmission, oil and gas production, petrochemical, and power industries to enhance reliability and cost-effective operation.*

*Dr. Smalley received a B.Sc. degree (Mechanical Engineering, 1963) and a Ph.D. degree (Mechanical Engineering, 1966) from the University of Nottingham in England. He is a Fellow of ASME and a member of the American Concrete Institute (ACI). He has published more than 100 technical papers and articles.*

## ABSTRACT

This paper presents the rotordynamic characteristics of a vertical submerged hydraulic turbine generator obtained during design, manufacturing, shop testing, and site testing. The hydraulic turbine

represents a new design with significant economic advantage in large LNG plants.

Described are the steps that were required by the Technical Advisor to assure that the hydraulic turbines would operate with acceptably low vibration levels. This verification process included two major rotordynamic analyses, a modal analysis of the turbine housing support, and shop testing at full load and full speed with cryogenic fluid.

Confirmed was that acceptable margins exist between predicted critical speeds and the wide operating speed range. The shop testing included a total of six hydraulic turbines (three with three stages, three with two stages). The rotordynamic evaluations were based on a two-level analysis with interaction of the flexible rotor and casing at the bearings and seals.

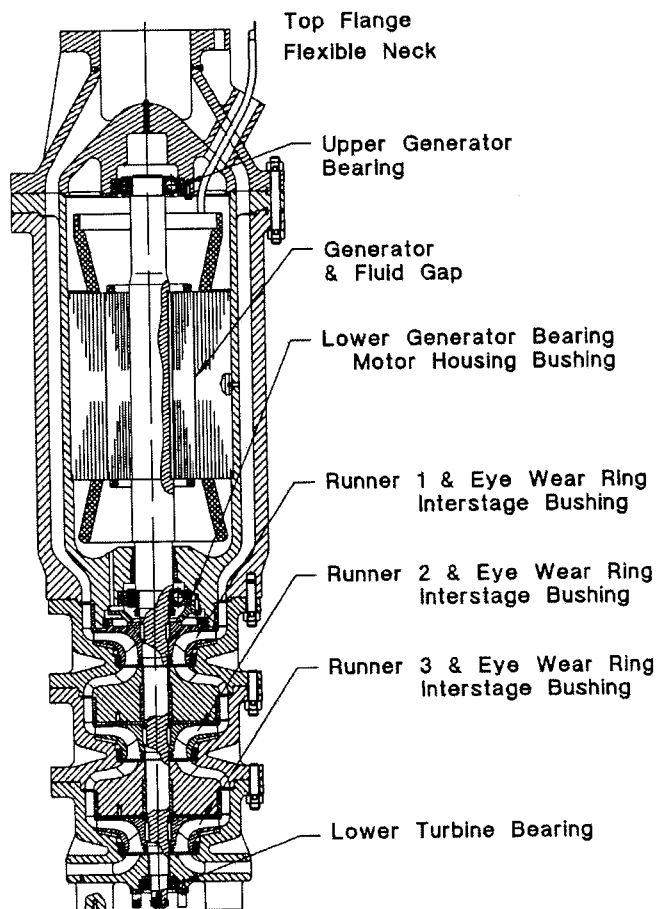
## INTRODUCTION

Vertical turbomachines, particularly pumps and liquid turbines, present a challenge in rotordynamic analysis and in shop testing. Darlow, et al. (1978), showed how the rotor, casing, and pump tank can interact dynamically in a single-stage vertical liquid metal pump. Two recent papers (Smalley, et al., 1998a, 1998b) addressed the complexities in predicting rotordynamic characteristics using the example of a five-stage vertical turbine. These two papers emphasized the importance of considering structural interaction between the rotor and its casing. Chang and Braun (1987) showed the necessity of considering a two-level model to reproduce an observed rotor instability in a vertical cryogenic pump. Childs (1978) presented a two-level stability analysis of the space shuttle main engine high-pressure fuel turbopumps, showing that the cantilevered casing and the rotor both participate in the first five modes.

This paper presents methods of tests and analysis which, together, provide assurance of reliability and integrity for a new machine of this type. These methods quantify component properties, determine critical speed margins, and document acceptability of vibration levels. To exemplify the methods, the paper addresses a series of vertical hydraulic turbines, which expand both heavy mix refrigerant (HMR) and liquefied natural gas (LNG) in a liquefied natural gas plant. The two-stage HMR turbine has an operating range of 32 to 45 bar (467 to 657 psi) for pressure, and 1050 to 1320 m<sup>3</sup>/hr (4623 to 5811 gpm) for flow. The three-stage LNG turbine has an operating range of 37 to 50 bar (540 to 730 psi) for pressure, and 750 to 1050 m<sup>3</sup>/hr (3302 to 4623 gpm) for flow.

Figure 1 shows the three-stage design. LNG flows downward from the top and expands via three radial inflow runners, which drive the liquid submerged generator through a common shaft. Three rolling element bearings support the rotor, one above the generator, one below the generator, and one at the bottom of the

turbine. All these bearings are lubricated and cooled by the cryogenic fluid. The casing supports each bearing. Rotor and casing also interact at the fluid gap between the generator and its stator, at the bushings between stages, and at wear rings on each turbine runner. The entire hydraulic turbine is mounted in a pressure vessel with inlet and discharge piping connections. The casing hangs from the upper flange and acts as a rigid body pivoting about this flange joint that connects the turbine to the heavy pressure vessel cover plate. The angular flexibility of this gasketed joint dominates the first mode of vibration for the rotor casing system. The test program included a modal analysis through a shaker test designed to verify a model developed for joint flexibility.



\* Approximate axial locations of accelerometers installed on casing.

Figure 1. Schematic of Three-Stage Turbine Generator.

The use of a hydraulic turbine in a refrigeration plant provides an alternative to a Joule-Thompson valve to expand high-pressure refrigerant. Expansion through a hydraulic turbine produces additional refrigeration, and provides electrical power as a further benefit.

A variable frequency generator allows efficient operation under varying flow and head conditions, but requires an operational speed range, free of resonance conditions (critical speeds), from 2500 rpm to 3600 rpm. In addition, since the generator may unexpectedly lose electrical load, a sudden acceleration will follow: the rotor responds to the unbalanced drive torque by accelerating to a maximum or "breakaway" speed (4200 rpm), where drive torque balances internal resistance torque. To provide satisfactory margins in accordance with international and API standards for all possible conditions, a target separation of 15 percent between any critical speed and the range from 2500 to 4200 rpm is required. The shop test program confirmed this separation margin. A paper by Habets and Kimmel (1999)

describes the requirements met during development of the hydraulic turbine.

Figures 2 and 3 show photographs of the turbine during installation prior to testing, and during disassembly after test.

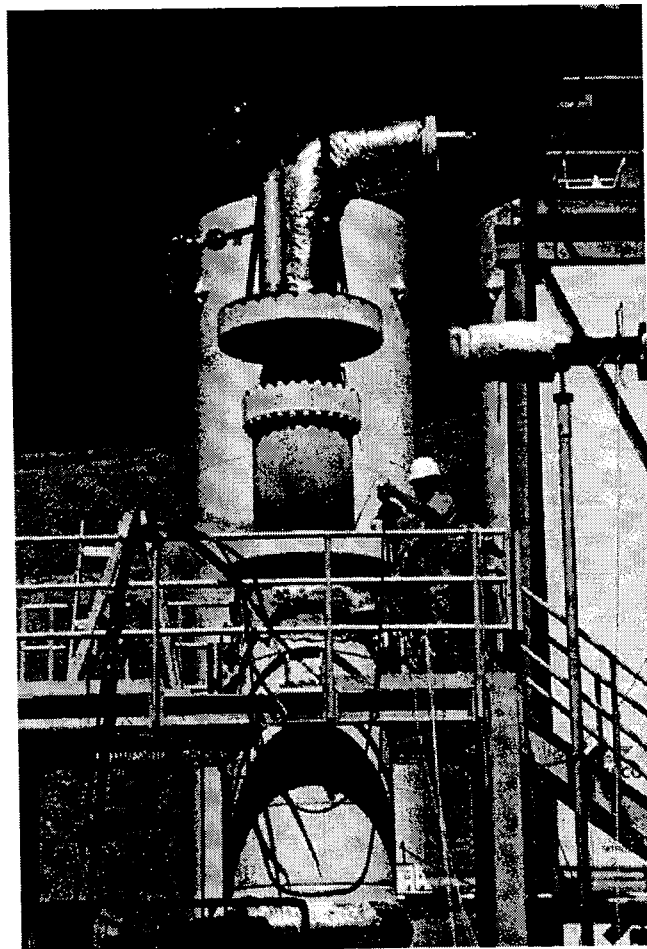


Figure 2. Turbine During Installation for Test.

#### UPPER FLANGE JOINT FLEXIBILITY

The turbine casing acts as a rigid body pivoting about the gasketed flange joint at its top, which for lateral rotordynamics, can deform under shear forces or under an applied lateral moment.

In addition to deformation of the gasket material and bolts, deformation of the flange material will introduce some additional flexibility, and the following relationship for an effective joint angular stiffness accounts for this additional flexibility of the flange metallic surface and body:

$$K_{joint} = 1 / (1/K_a + 1/K_{flange}) \quad (1)$$

whereby  $K_a$  represents the angular stiffness for the gasket and bolts (refer to APPENDIX A). Shear deformation of the gasket yields the following simple relationship for shear stiffness:

$$K_s = \frac{A_g G_g}{t} \quad (2)$$

where  $A_g$  is the gasket sheared area,  $G_g$  is the gasket material shear modulus, and  $t$  is the gasket thickness.

Testing was carried out to verify the modeling approach and to remove uncertainties and simplifications in the model. With the complete turbine in place, a shaker mounted to the turbine casing applied a variable frequency exciting force. Accelerometers on the

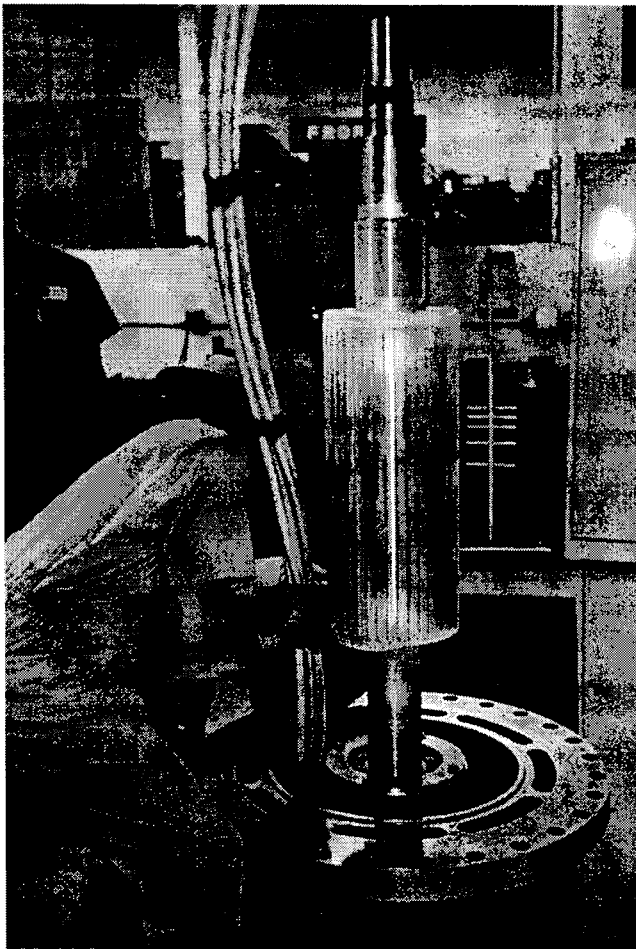


Figure 3. Rotor During Disassembly for After-Test Inspection.

turbine casing measured vibration, supplemented by an accelerometer on the heavy mounting plate above the turbine. Measurements were carried out with the turbine cold and full of LNG. Figure 4 shows two resonant peaks (15.6 Hz, 28.1 Hz) in the bottom accelerometer’s response. Table 1 summarizes modal information, and Figure 5 presents an approximate display of the modal data. The lower mode at 15.6 Hz has significant participation of the heavy support plate, suggesting a structural resonance of the test stand. In the second mode, the turbine casing pivots about the flange joint. A simple beam model of the casing, connected by angular *and* translational stiffness to a rigidly fixed top support plate, predicts a resonant frequency of 37 Hz, using  $8.82 \times 10^8$  N.m/radian ( $7.80 \times 10^9$  lb.in/radian) for angular stiffness (based on the model in APPENDIX A). The mode shape of the simple beam model under these conditions is identical to the mode shape measured at 28.1 Hz of the actual hydraulic turbine. The simple beam model also indicates that the expected translational stiffness does not influence the frequency of this angular mode.

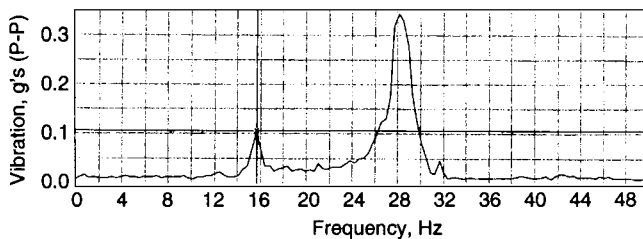


Figure 4. Representative Response Spectrum for Three-Stage Turbine Generator (Accelerometer at Bottom of Casing).

Table 1. Modal Phase and Amplitude Information.

Location	15.6 Hz Mode		28.1 Hz Mode	
	Relative Amplitude	Phase Degrees	Relative Amplitude	Phase Degrees
Top	0.3	180	0.03	0
Middle	0.3	0	0.48	1.1
Bottom	1	0	1.0	0

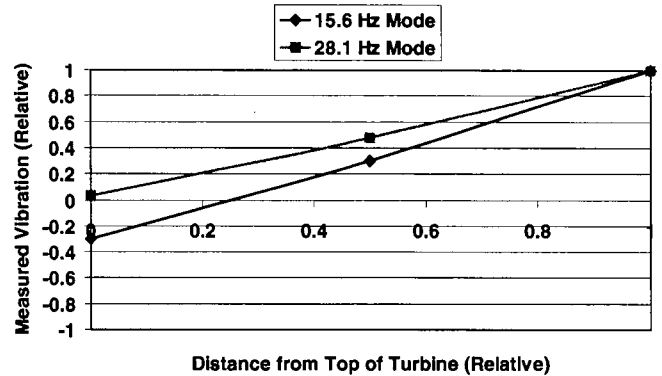


Figure 5. Casing Mode Shapes from Shaker Modal Tests.

The measured resonant frequencies for the turbine when empty at ambient temperature and when filled with cold LNG differ by less than 3 percent (28.9 Hz and 28.1 Hz, respectively). This small difference indicates insensitivity of the joint stiffness to any changes in compression or material compliance with temperature.

Mounting the turbine directly from the support plate (*with no gasket*) produced a measured resonant frequency of 41 Hz with a similar mode shape (pivoting about the flange joint). Comparing this 41 Hz with the 37 Hz predicted with the gasket/bolt stiffness of  $8.82 \times 10^8$  N.m/radian ( $7.80 \times 10^9$  lb.in/radian) suggests the metal surface and flange body have an effective angular stiffness of  $1.03 \times 10^9$  N.m/radian ( $9.10 \times 10^9$  lb.in/radian). Adding the gasket/bolt stiffness in series with this stiffness for metal surface and flange body produces a net joint stiffness of  $4.75 \times 10^8$  N.m/radian ( $4.20 \times 10^9$  lb.in/radian) according to Equation (1), and a predicted natural frequency of 27.1 Hz—close to the measured value of 28.1 Hz. The half power point method applied to the measured response indicates a damping ratio of 2.7 percent for the rigid body resonance.

The modal test program provides an empirical confirmation of the gasket/bolt stiffness model, a value to use for the additional metallic stiffness in series with the gasket, and an effective damping ratio for joint deflection. The elastic restraint imposed by the bolts dominates the joint stiffness (refer to APPENDIX A). Figure 6 demonstrates this by presenting predicted net angular stiffness of the joint as a function of bolt preload, accounting for nonlinear stiffening of the gasket material (by a factor of three over this preload range). The stiffness changes very little, indicating the gasket predominantly provides compressive strength to keep the bolts in preloaded contact with the flange itself.

PREDICTED CRITICAL SPEEDS

Figure 7 shows the three-dimensional finite element model of the turbine casing structure that is connected at its top to “ground” via the angular and shear stiffnesses discussed above ( $4.75 \times 10^8$  N.m/radian;  $4.91 \times 10^9$  N/m ( $4.20 \times 10^9$  lb.in/radian;  $2.80 \times 10^7$  lb.in/radian), respectively), with 2.7 percent damping ratio. Figure 8 shows a rotor bending model, with added mass, polar, and transverse, inertias at the generator and turbine runners, connected to the casing structure at bearings, bushings, and wear rings.

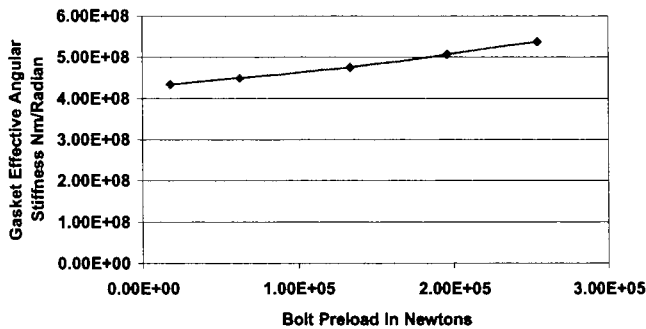


Figure 6. Predicted Angular Stiffness as a Function of Bolt Preload.

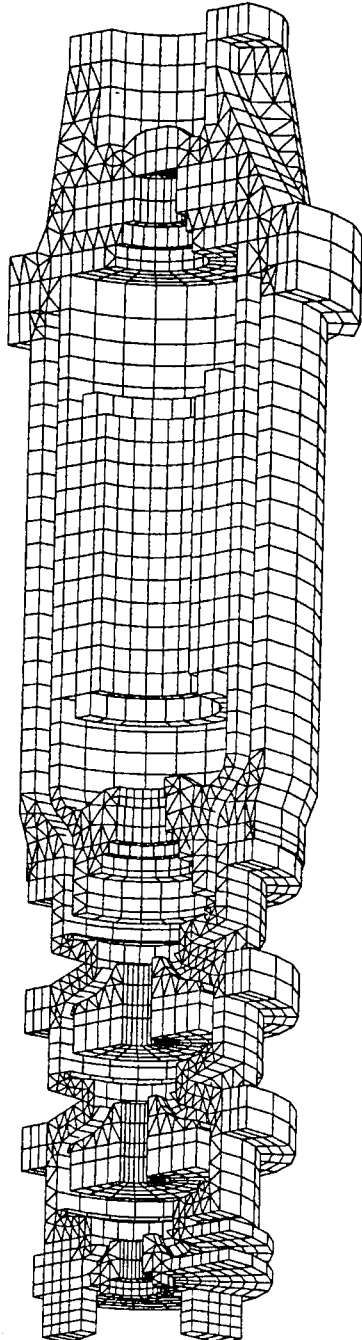


Figure 7. Three-Dimensional FE Model of Casing.

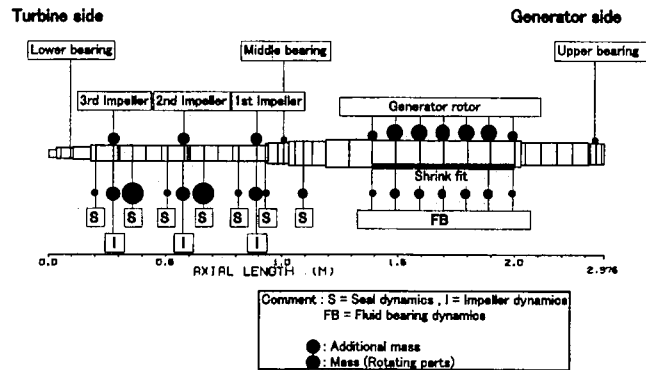


Figure 8. Model of Analyzed Rotor.

The rotor system model includes seal forces, impeller forces, bearing forces, and forces from the fluid filled gap between the generator rotor and stator. The impeller stiffness, damping, and inertia coefficients are based on the book *Turbomachinery Rotordynamics* by Childs (1993). The seals are analyzed using a turbulent Reynolds equation solution, accounting for inlet hydrostatic effects. Stiffness coefficients for the rolling element bearings are calculated by an equilibrium model which accounts for Hertzian deformation of the balls. The generator fluid gap is analyzed as a turbulent bearing to obtain stiffness and damping coefficients, and the gap fluid inertia coefficients are predicted by the method of Reinhardt and Lund (1975); since the fluid gap has a series of axial grooves, effective values for clearance and length are used in these calculations.

Figure 9 shows a typical predicted unbalance response of the rotor relative to the casing at the generator midpoint. The unbalance (4W/N), in accordance with API, is distributed along the rotor's length. The response has a clear resonance at 4800 rpm with 275 microns (10.8 mils) peak-to-peak amplitude. A barely perceptible resonance, at 1500 rpm, involves the casing and turbine rotor moving together, and pivoting about the upper flange joint.

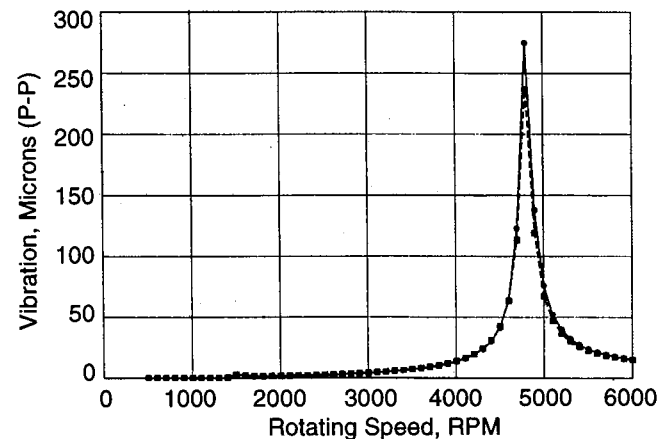


Figure 9. Predicted Vibration at Generator Midpoint Relative to the Casing as a Function of Speed.

Figure 10 shows the predicted vibration of rotor relative to the casing at the location of the uppermost (TEM) runner as a function of speed under the same unbalance distribution as for Figure 9. This runner experiences the highest level of resonant vibration in the turbine section, reaching 115 microns (4.5 mils) peak-to-peak at 4800 rpm, but this turbine vibration is lower than the generator vibration by a factor of 2.5.

Figure 11 shows the predicted absolute vibration response for the casing at 4800 cycles per minute (cpm), with a maximum amplitude of 149 microns (5.9 mils) at the bottom of the casing,

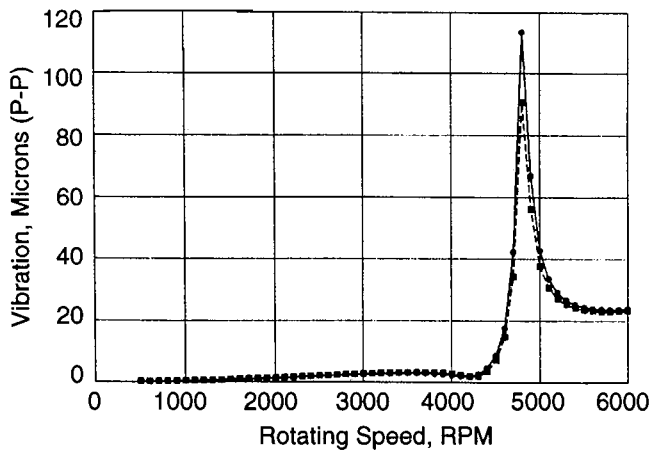


Figure 10. Predicted Turbine Maximum Vibration Relative to the Casing as a Function of Speed.

and about 70 microns (2.8 mils) amplitude at the midpoint of the casing. A 70-micron (2.8-mil) midcasing amplitude at 4800 cpm implies a velocity of 12.44 mm/sec (0.49 ips) rms.

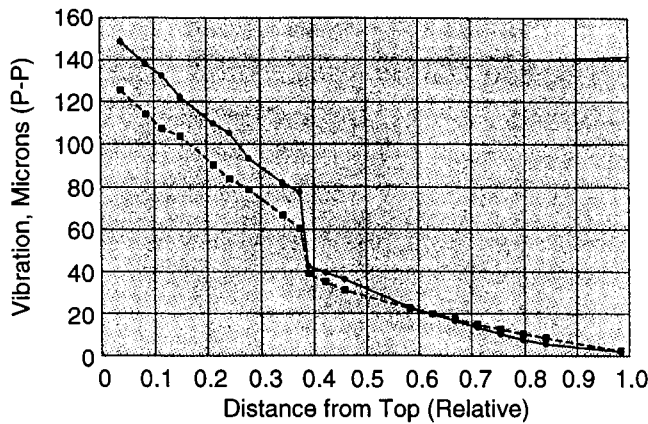


Figure 11. Predicted Absolute Casing Vibration Response at 4800 CPM.

### SHOP TESTING UNDER CRYOGENIC CONDITIONS

Operating tests in LNG are to confirm performance and mechanical behavior, specifically separation margins between the operating speed range and critical speed. Tests are carried out with the generator inactive (minimum torque load on the turbine), and with the generator active (full torque load on the turbine). Accelerometers were mounted at two locations on the turbine housing during the tests.

Figure 12 presents casing vibration measured with the accelerometer at approximately the midpoint of the casing. The speed range covers 1000 to 4900 rpm, and measurements are for all three of the three-stage turbines (generator inactive). All vibrations follow a remarkably similar variation with speed, and reach 12.9 mm/sec (0.51 ips) rms at 4900 rpm (close to the calculated resonant level of 12.44 mm/sec (0.49 ips) rms based on Figure 11). For speeds up to 4500 rpm, the vibration appears to follow a parabolic increase with speed. Linear regression between vibration and speed squared produces the solid line shown in Figure 12 (with standard error of 0.62 mm/sec (0.024 ips) and regression coefficient ( $R^2$ ) of 88 percent). These regression parameters for the entire data set confirm the relative consistency of all three turbines. For all turbines, vibration levels at 4900 rpm clearly lie well above the square law line fitted to the lower speed points, which suggest that resonance dominates the vibration magnitude at 4900 rpm. No data are available to confirm the speed of maximum vibration, but

this figure suggests that the critical speed lies at or above 4900 rpm. Figure 13 shows vibration levels for the same three turbines, with the generator active, on the same scale as Figure 12, demonstrating significantly lower vibrations under loaded conditions (maximum vibration less than 3 mm/sec (0.12 ips) rms). The data for generator active includes six or more data points at each speed, covering a range of flow and head conditions. These data cover all three LNG turbines and the vertical scatter indicates the extent to which vibration varies with flow at constant speed.

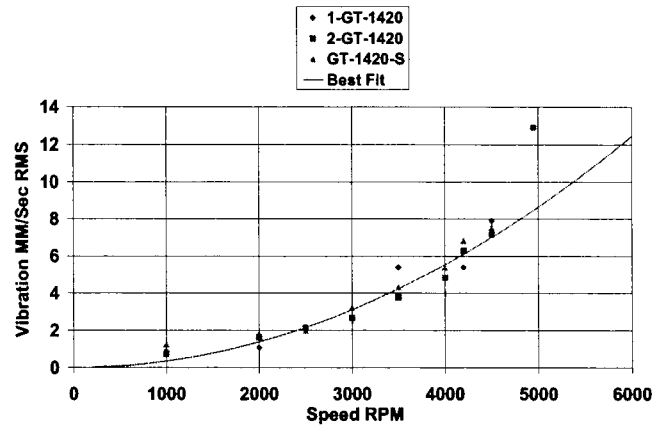


Figure 12. Plot of Measured Casing Vibration Versus Speed for All Three Three-Stage Turbines—Inactivated.

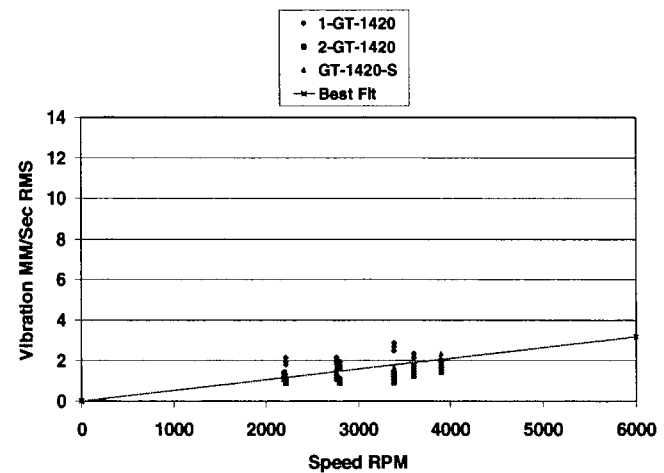


Figure 13. Plot of Measured Casing Vibration Versus Speed for All Three Three-Stage Turbines—Activated.

Figures 14 and 15 show very similar vibration characteristics for the two-stage turbine generator. Linear regression with speed squared up to 4500 rpm for the generator inactive produces a standard error of 0.67 mm/sec (0.026 ips), and a regression coefficient ( $R^2$ ) of 83 percent—indicating very similar dependence with speed to the three-stage unit. The two-stage regressed line lies about 2 mm/sec (0.079 ips) below the three-stage line at 4500 rpm. With the generator activated (Figure 15), the two-stage turbine again exhibits lower vibrations than under inactivated conditions, but by a smaller margin. The two-stage units exhibit somewhat more scatter when loaded, but the highest recorded vibration under activated conditions remains below 4.5 mm/sec (0.18 ips) rms. The value of 4.5 mm/sec (0.18 ips) rms was the test acceptance criteria.

### SITE VIBRATION TESTING

Following shop testing, the turbines were delivered and installed at site. Once the plant was operational, some vibration data were acquired at prevailing conditions of speed and flow, using the

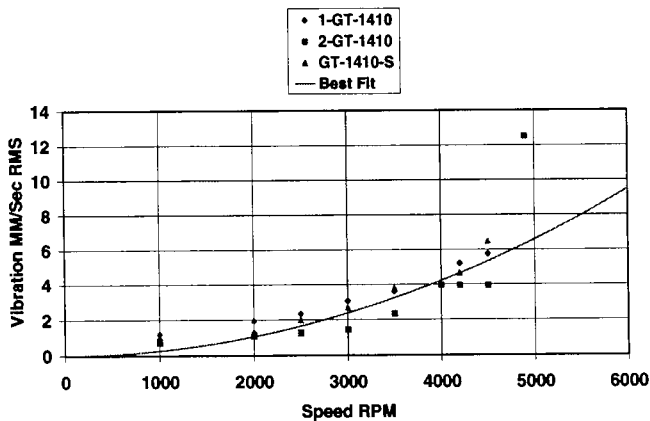


Figure 14. Plot of Measured Casing Vibration Versus Speed for All Three Two-Stage Turbines—Inactivated.

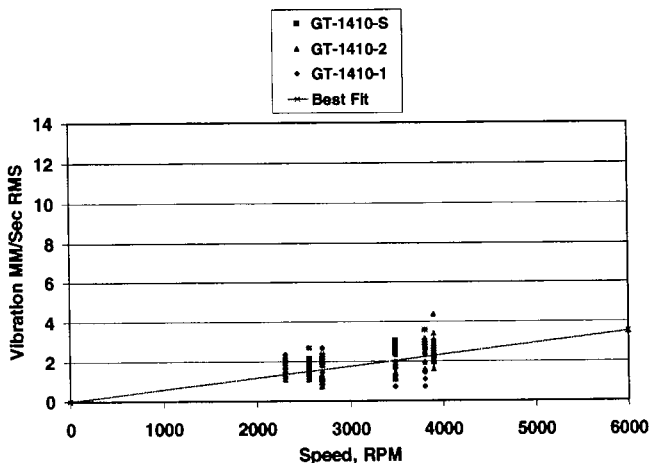


Figure 15. Plot of Measured Casing Vibration Versus Speed for All Three Two-Stage Turbines—Inactivated.

installed instrumentation. Figures 16 and 17 compare minimum and maximum vibrations from the site data with the most relevant corresponding shop test vibration data for the two- and three-stage units. The speed ranges were limited for the site data, as shown on these figures, and for some units only a single speed was recorded. The shop data presented in these figures are selected to match the speed range of the site data for the units in question. The site vibrations are generally similar to or a little higher than the shop tests data, but in all cases remain well below the shop acceptance level.

DISCUSSION OF RESULTS

The results presented in the preceding sections of this paper indicate the value of tests, for quantifying both component and system characteristics. They also provide encouraging confirmation of the predictive methods used during design and analysis of this vertical hydraulic turbine. In addition, the fact that the site tests remain well below the shop test acceptance level confirms the predictive value of the shop tests for this equipment.

The consistency of vibration level across the six hydraulic turbines confirms that manufacturing, assembly, and balancing to a particular grade level result in a consistent level of mass eccentricity in the rotor.

The effect of loading by activating the generator most likely introduces magnetic forces that change contact conditions at rolling element bearings, rotor axial position, seal eccentricities, and pressure differentials across seals. It may also cause some change in hydraulic unbalance. The apparent stiffening of the system under load reduces vibration below 3600 rpm by almost a

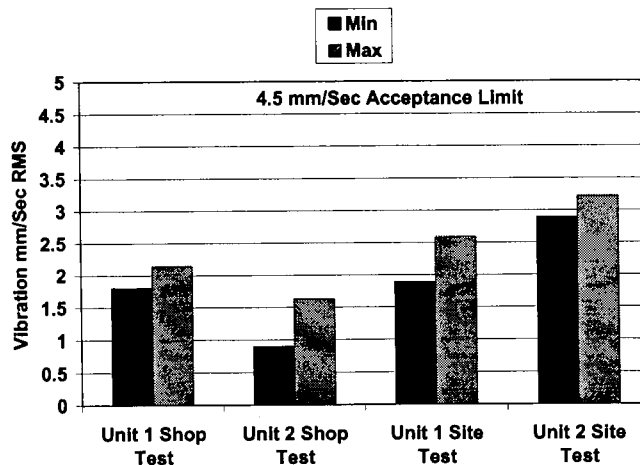


Figure 16. Comparison of Shop and Site Test Vibrations for Two-Stage Turbines at 2700 RPM.

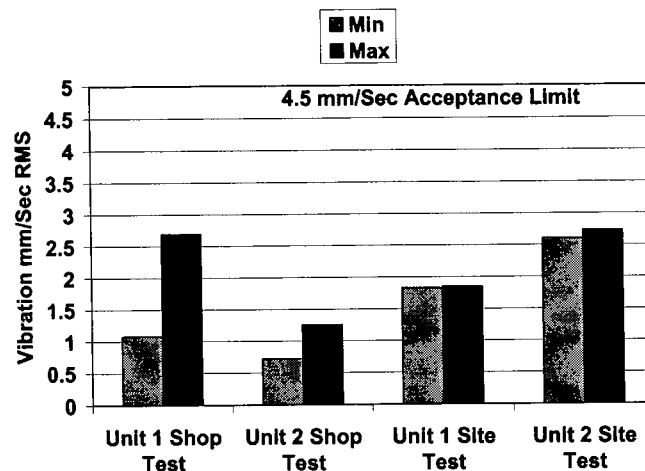


Figure 17. Comparison of Shop and Site Test Vibration for Three-Stage Turbines at 2400 to 2800 RPM.

factor of 2 for the three-stage unit, and by 25 percent for the two-stage unit. This effect of loading is discussed by Madison (2000).

Five of the six hydraulic turbines indicate purely synchronous vibration consistent with the effects of unbalance, but just one of the three-stage units exhibited vibration at a slightly subsynchronous frequency (4200 cpm) when running above 4500 rpm. Possible causes of such a phenomenon include: rotating friction at interference fits, a flow instability, or magnetic effects of the fluid submerged generator. Maximum vibration levels for this turbine remained the same as for the others. The fact that the phenomena occurred only at a speed outside the normal operating range, and even so did not appear harmful, precluded further investigation of this phenomenon.

Monitoring the no-load characteristics of cryogenic turbines proves to be a powerful diagnostic method as presented in a paper recently published (Habets, 2000).

Shaft vibration was not measured during the tests. As an alternative, scaling predicted shaft vibrations by the ratio of measured to predicted casing vibrations, offers an approximate means to infer shaft motion in the test stand. The predicted casing vibrations of Figure 11 correspond to the measurement location of Figure 12, and are driven by the same unbalance excitation used to predict generator rotor vibration, and the first runner vibration in Figures 9 and 10 (with predicted maximum values of 275 and 115 microns (10.8 and 4.5 mils), respectively). The measured maximum casing vibration of 12.9 mm/sec (0.51 ips) rms in Figure 12, at 4900 rpm, almost directly equals the predicted maximum

casing vibration of 12.44 mm/sec (0.49 ips) rms in Figure 11, at the generator critical speed, suggesting a scaling factor of 1.04 for maximum vibrations. This factor yields 285 and 119 microns (11.2 and 4.7 mils), respectively, for inferred maximum vibration of generator and first impeller at the highest speed in the test stand. These vibrations represent 11 percent of the generator fluid gap (2700 microns (106 mils)) and 46 percent of the low end of the tolerance range for the smallest turbine seal clearance (260 microns (10.2 mils)). Review of the predicted and measured variation of vibration with speed confirms that the generator and turbine vibrations at all lower speeds will lie even further below any seal clearance limit. Tear down of one turbine following the performance and vibration tests showed no damage at any seals, helping to confirm the above inferences.

The maximum casing vibration under loaded conditions within the operating speed range for two- or three-stage turbine shop tests lies below 4.5 mm/sec (0.18 ips) rms, i.e., just over one-third of the resonant value at 4900 rpm. Scaling shaft vibrations to this lower casing vibration suggests the maximum vibration during loaded operation remains below 15 percent of the smallest seal clearance.

## METHODOLOGIES APPLIED

The demonstration of rotordynamic integrity in this paper illustrates a number of methods for test and analysis of vertical pumps and turbines for cryogenic applications:

- Gasket angular stiffness modeling
- Modal shaker testing to confirm gasket component properties
- Coupled rotor-casing dynamic modeling to predict system dynamic characteristics
- Shop vibration testing under cryogenic conditions
- Overspeed testing for loss of load critical speed margins
- Inferential analysis of shaft vibration levels
- Post test inspection
- Confirmatory site vibration testing

An important challenge to which this paper implicitly addresses itself is to introduce new technologies (such as these turbines), which reduce capital costs and improve operational efficiencies, while managing risk for critical plants. The overall series of steps in which the above methods were applied help address this challenge. While listed sequentially above, some of these steps involved interaction and iteration.

Early predictions of system characteristics focused attention on critical elements, particularly the gasket angular stiffness, which if too high could have pushed a structural mode into the running speed range. The development of a model for this component, the confirmation of this model through shaker testing, the inferred gasket damping, and the predicted structural resonance at 1500 cpm, using this model helped set this concern to rest.

One of the differences between pump and turbine applications of this rotor configuration is the need to consider loss of load for turbines. This makes the required range of operating speeds without a critical speed much wider than for a pump. The early system predictions also showed the need to minimize the bearing span and maximize stiffness of the generator shaft in order to give a satisfactory margin between maximum speed under loss of load and the first generator critical speed. The final configuration reflects such optimization, and an important focus of the vibration testing under cryogenic conditions is to document the predicted margin. Running under no load to a speed 36 percent above the normal maximum of 3600 rpm demonstrated the vibrations still rising toward a critical speed at or above 4900 rpm.

A further challenge encountered in almost all turbomachinery is to ensure a satisfactory margin from rubbing under high vibration at close clearance locations, such as seals and wear rings. Since measurement of vibrations is not economically possible at every such seal, a requirement exists to make inference from vibration

measurements remote from the close clearance location. In many compressor applications, the remote location is at the fluid film bearings, which support the rotor. However, in these cryogenic pumps (and in many gas turbines), the closest vibration measurement is a casing-mounted accelerometer. Without direct measurement, an inferential process is required to provide assurance that rubbing will not occur. This inferential process anchors and normalizes the model predictions at a common point where both predicted and measured data are available; it then assumes validity of the predicted mode shape to infer vibration at other locations where no measurements are available. The preceding discussion of results describes the inferential process as applied to this turbine. The margins are sufficiently high to make any inaccuracies of the inferential process tolerable. Lack of evidence of any contact between rotating and stationary close clearance components during teardown and inspection after the tests confirms this inference. The addition of site vibration data that remains well below the acceptance level for shop testing provides further confirmation that the preceding combination of test and design analysis will successfully assure rotordynamic integrity of a new machine.

The design, analysis, evaluation, and test methods should readily apply to pumps as well as turbines and to other liquids. The method of construction illustrated in Figure 1 has been applied to many pumps for various fluids including:

- Propylene (cryogenic and supercritical)
- Propane (warm pressurized and cryogenic)
- Methane
- Nitrogen
- Ethane
- Ethylene (cryogenic and supercritical)
- Butane and isobutane
- Anhydrous ammonia

The configurational differences between a motor driven pump and a hydraulic turbine driving a generator are small, and are likely to have only a small influence on rotordynamics. The flow is in the opposite direction, but the pressures acting across seals and impellers are similar in magnitude and direction. The bearings see nominally similar loads. The motor is submerged, just like the generator, and is likely to experience similar fluid-film forces. When operating against a low flow resistance, the pump would be expected to experience loading similar to the turbine when inactive, with similarly higher vibration than when fully loaded.

The facilities used for the hydraulic turbine shop test have also been used for the testing of pumps. The benefits of performing a shop test are the ability to control conditions, independent of plant operation. Shop testing allows the range of loads from inactive to fully loaded, and a range of speeds beyond those likely to occur at site (except under an upset loss of load for the turbine). Based on the shop test results, the inactive conditions lead to the highest vibrations. These inactive conditions probably allow the clearest evaluation of the rotordynamics model, but if testing is limited to site ("production") testing under plant prevailing loads, the vibrations will be most representative of expected operation.

The turbine design, in addition to the LNG and HMR addressed here, is being considered for turbine applications involving other fluids, including:

- Nitrogen
- Ethane
- Ethylene
- Propane

While not all plants have such stringent demands for reliability, some combination of the methods discussed should be cost-effective for use in a wide range of applications.

## CONCLUSIONS

- A combined program of analysis and test can be highly effective in assuring the rotordynamic integrity of a new machine.
- The measured rigid body natural frequency of the casing structure confirms predictions of the model presented for gasket angular stiffness.
- The predicted separation margins between highest possible speed and the first rotor critical speed have been satisfactorily confirmed by the tests.
- The predictions of vibration amplitude are in satisfactory agreement with predictions.
- When loaded, the turbine vibration is distinctly lower than when unloaded.
- The consistency of vibration levels for different turbines indicates consistency in manufacturing and assembly.
- Inferred rotor vibrations lie well below minimum seal clearances within the operating speed range, and up to maximum speed under loss of load.

## APPENDIX A

Assuming an effective Young's Modulus for normal compression of the gasket material, the following integral gives the inplane reaction moment caused by an imposed angular deformation of the gasket:

$$M = \frac{E_g \alpha}{t} \int_{r_i}^{r_o} \int_0^{2\pi} r^3 \cos \theta d\theta dr \quad (\text{A-1})$$

Evaluating the integral, subtracting bolt hole area, and accounting for bolt stretch gives an angular stiffness for the gasket and bolts as follows:

$$K_a = \left( \frac{E_g \pi}{4t} \right) \left( r_o^4 - r_i^4 \right) - \frac{E_g A_b}{2t} r_b^2 N_b + \frac{E_b A_{root}}{2L_b} R_b^2 N_b \quad (\text{A-2})$$

where:

- M = Reaction moment of the gasket in response to angular deflection of one surface relative to the other
- $E_g$  = Gasket effective Young's Modulus (276 MPa (4.00 × 10<sup>4</sup> psi))
- $\alpha$  = Angle of deflection of one metal flange surface relative to the other
- t = Gasket thickness (3.175 mm (0.125 in))
- $r_i, r_o$  = Inner and outer radii of the gasket (162 mm, 279 mm (6.38 in, 10.98 in))
- $\theta$  = Angular coordinate of an elemental area of the gasket
- $K_a$  = Angular stiffness of the gasket and bolts (8.82 × 10<sup>8</sup> N.m/radian (7.8 × 10<sup>9</sup> lb.in/radian))
- $A_b$  = Area of gasket cut out for a bolt (958 mm<sup>2</sup> (1.48 in<sup>2</sup>))
- $R_b$  = Bolt pitch radius (244 mm (9.61 in))
- $N_b$  = Number of bolts (16)
- $K_s$  = Gasket shear stiffness
- $G_g$  = Gasket material shear modulus (106.2 MPa (1.54 × 10<sup>4</sup> psi))
- $A_{root}$  = Bolt root area (591 mm<sup>2</sup> (0.916 in<sup>2</sup>))
- $L_b$  = Bolt effective length (101.2 mm (3.98 in))
- $E_b$  = Bolt Young's Modulus (2.0 × 10<sup>5</sup> MPa (2.90 × 10<sup>7</sup> psi))

And values in parentheses indicate specific values for the joint in question.

## REFERENCES

- Chang, C. M. and Braun, F. W., 1987, "Solving the Vibration Problem of a Vertical Multistage Cryogenic Pump," *Proceedings of the Fourth International Pump Symposium*, Turbomachinery Laboratory, Texas A&M University, College Station, Texas, pp. 85-95.
- Childs, D. W., 1978, "The Space Shuttle Main Engine High-Pressure Fuel Turbopump Rotordynamic Instability Problem," *Journal of Engineering for Power*, 100, pp. 48-57.
- Childs, D. W., 1993, *Turbomachinery Rotordynamics—Phenomena, Modeling, and Analysis*, New York, New York: John Wiley & Sons, Inc.
- Darlow, M. S., Smalley, A. J., and Ogg, J., June 1978, "Critical Speeds and Response of a Large Vertical Pump," Joint ASME/CSME Pressure Vessels & Piping Conference, Montreal, Canada, ASME Paper No. 78-PVP-34.
- Habets, G. L. G. M., March 2000, "Monitoring Cryogenic Turbines Using No-load Characteristics," Eighth International Symposium on Transport Phenomena and Dynamics of Rotating Machinery, ISROMAC-8, Honolulu, Hawaii.
- Habets, G. L. G. M. and Kimmel, H. E., April 1999, "Development of a Hydraulic Turbine in Liquefied Natural Gas," *Proceedings of the Seventh International Fluid Machinery Conference*, IMechE, The Hague, The Netherlands.
- Madison, J., March 2000, "Torque Dependent Vibrations for a Vertical Cryogenic Turbine Generator," *Proceedings of the Eighth International Symposium on Transport Phenomena and Dynamics of Rotating Machinery*, ISROMAC-8, I.
- Reinhardt, E. and Lund, J. W., April 1975, "The Influence of Fluid Inertia on the Dynamic Properties of Journal Bearings," *Journal of Lubrication Technology*, pp. 159-167.
- Smalley, A. J., Hollingsworth, J. R., Habets, G. L. G. M., and Kimmel, H. E., May 1998a, "Rotor Dynamic Analysis of a Cryogenic Submerged Turbine Generator," *Proceedings of the Nineteenth Southeastern Conference on Theoretical and Applied Mechanics*, SECTAM XIX, Deerfield Beach, Florida, pp. 708-718.
- Smalley, A. J., Hollingsworth, J. R., Habets, G. L. G. M., and Kimmel, H. E., September 1998b, "Rotor Dynamic Analysis of a Submerged Turbine Generator Driven by Liquefied Natural Gas," *Proceedings of the Fifth International Conference on Rotor Dynamics*, IFToMM, Darmstadt University of Technology, Darmstadt, Germany, pp. 298-309.

## ACKNOWLEDGEMENTS

The authors wish to acknowledge the contribution of Shell International Oil Products B.V., EBARA International Cryodynamics, and Southwest Research Institute (SwRI) for their support and encouragement of this paper; Joel Madison of EBARA who managed the design, analysis, manufacture, and testing of these turbines, and acquired much of the shop and site test data; Ralph Harris of SwRI who performed the test and analysis of gasket flexibility; and Justin Hollingsworth of SwRI who performed much of the early rotordynamics analysis.